Development of a Multichannel Vestibular Prosthesis Prototype by Modification of a Commercially Available Cochlear Implant

Nicolas S. Valentin, Kristin N. Hageman, Chenkai Dai, Charles C. Della Santina, and Gene Y. Fridman, *Member, IEEE*

***Abstract*—No adequate treatment exists for individuals who remain disabled by bilateral loss of vestibular (inner ear inertial) sensation despite rehabilitation. We have restored vestibular reflexes using lab-built multichannel vestibular prostheses (MVPs) in animals, but translation to clinical practice may be best accomplished by modification of a commercially available cochlear implant (CI). In this interim report, we describe preliminary efforts toward that goal. We developed software and circuitry to sense head rotation and drive a CI's implanted stimulator (IS) to deliver up to 1 K pulses/s via nine electrodes implanted near vestibular nerve branches. Studies in two rhesus monkeys using the modified CI revealed *in vivo* performance similar to our existing dedicated MVPs. A key focus of our study was the head-worn unit (HWU), which magnetically couples across the scalp to the IS. The HWU must remain securely fixed to the skull to faithfully sense head motion and maintain continuous stimulation. We measured normal and shear force thresholds at which HWU-IS decoupling occurred as a function of scalp thickness and calculated pressure exerted on the scalp. The HWU remained attached for human scalp thicknesses from 3–7.8 mm for forces experienced during routine daily activities, while pressure on the scalp remained below capillary perfusion pressure.**

***Index Terms*—Cochlear, dizziness, electrical stimulation, implant, prosthesis, vestibular.**

I. Introduction

THE VESTIBULAR labyrinth helps maintain gaze and postural stability by driving reflexive eye and body movements in response to head motion. Rotational head motion is normally encoded into vestibular nerve activity by six semicircular canals (SCCs), three in each inner ear, which modulate afferent neuron firing rates. Damage to sensory hair cells in the SCCs can occur due to infection, Ménière's disease or ototoxic medications, causing impairment of vestibular reflexes. The resulting disequilibrium, blurred vision during head movements, and postural instability degrade quality of life and increase risk of injury due to falls [4].

There is currently no adequate treatment for individuals with bilateral vestibular hypofunction (BVH) who fail to improve despite vestibular rehabilitation exercises. Preclinical studies in rodents and nonhuman primates strongly suggest that a multichannel vestibular prosthesis (MVP) could improve quality of life for such patients [5]–[12].

Significant effort has been directed toward reducing the physical size of the sensors and the signal processing hardware of the vestibular prosthesis with the intent to develop a fully implantable device [10], [11], [18], [39]–[41]. However, considering the large capital investment and regulatory burden required to create a new implantable stimulator de novo, translation to clinical practice may be best accomplished by modification of a commercially available cochlear implant (CI) system. Initial attempts at prosthetic vestibular stimulation in humans using cochlear implant (CI) stimulators have revealed promising preliminary results [13]–[16], [37], [38]. While these stimulation experiments successfully confirmed the ability of a CI to evoke the intended response of the vestibular nerve via patterned stimulation delivered to custom electrodes, they did not address the overall design that would enable a CI to be used as a vestibular implant. For a CI to function as a vestibular prosthesis, the system would need the ability to not only stimulate the nerve, but also to sense head rotation velocity in 3-D, process the data and modulate the stimulation pattern delivered to each of the three branches of the nerve in real time, and be self-contained and compact so that it could be worn by a patient. A more complete system design that would adapt a commercial CI to function as a vestibular prosthesis could expedite translating research findings into clinical use by overcoming significant technological and regulatory hurdles.

We adapted a commercially available CI system to function as a semi-implantable MVP. Our design includes motion sensors and a power source coupled magnetically to a modified CI's implanted stimulator (IS) analogous to a method suggested in a patent publication by Garnham *et al.* [36]. Using a CI to implement a complete vestibular prosthesis presents a unique challenge. Unlike a CI, an MVP uses gyroscopes to accurately sense skull rotation in 3-D. Consequently, transcutaneous magnetic (mechanical) coupling between the external head-worn component that contains the gyroscopes and the magnetically coupled implant must withstand head movements encountered during normal daily activities (e.g., walking, jogging, climbing

Manuscript received September 20, 2012; revised January 21, 2013 and March 13, 2013; accepted April 08, 2013. Date of publication May 01, 2013; date of current version September 04, 2013. This work was supported by the National Institute on Deafness and Other Communication Disorders (NIDCD)under Grant R01DC009255 and Grant 1F31DC010099-01A1.

The authors are with the Johns Hopkins Vestibular NeuroEngineering Lab, Department of Otolaryngology-Head & Neck Surgery and Biomedical Engineering, Johns Hopkins School of Medicine, Baltimore, MD 21205 USA (e-mail: gfridma1@jhmi.edu).

Color versions of one or more of the figures in this paper are available online at http://ieeexplore.ieee.org.

Digital Object Identifier 10.1109/TNSRE.2013.2259261

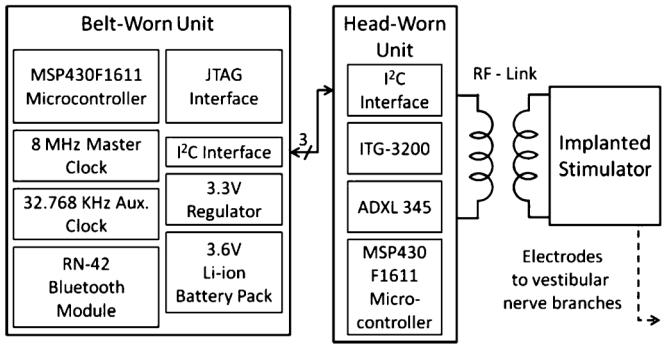

Fig. 1. Modified cochlear implant circuit block diagram. Our MCI prototype consists of 1) the BWU, 2) the HWU, and 3) the IS. The BWU samples sensors on the HWU every 5 ms and calculates instantaneous rate of stimulation. Pulse commands are sent to the HWU and relayed via radio frequency to the IS, which delivers frequency-modulated biphasic charge-balanced pulses to the vestibular nerve. Power is provided by a +3.3 V supply, drawn from a 3.6 V Li-ion battery pack housed in the BWU.

stairs), which can include head rotations with peak velocities up to $\sim 400^\circ/\mathrm{s}$ and accelerations up to $\sim 11500^\circ/\mathrm{s}^2$ (although the vast majority of head movements are much slower) [17]. At the same time, forces on the intervening scalp must not exceed the safety criteria indicated by the capillary perfusion pressure.

We describe our design of the modified CI (MCI), system bench tests and animal experiments, and we examine the technical challenge of maintaining a safe but strong transcutaneous magnetic coupling between the head-worn unit (HWU) and the IS. Our findings highlight factors that must be considered in development of an MCI intended to maintain uninterrupted vestibular nerve stimulation.

II. Device Description

A. System Overview

As shown in Fig. 1, the MCI prototype comprises three main components: a belt-worn unit (BWU), an external HWU and an IS. The BWU provides power to the HWU and reads head motion information from gyroscopes and linear accelerometers in the HWU via I2C. Based on the gyroscope measurements, the BWU determines the instantaneous stimulation pulse-rate for each electrode, schedules and sends a command to the HWU to deliver each pulse. The HWU relays the pulse information via the radio-frequency (RF) link to the IS. IS in turn delivers each specified electrical current pulse to the vestibular nerve via one of the nine electrodes implanted in the labyrinth. Under normal operating conditions, the MCI draws 21.1 mA from a regulated 3.3 V supply. The IS consumes 11.4 mA and the BWU+HWU consumes 9.7 mA.

B. Belt-Worn Unit

The BWU holds two 3.6 V lithium-ion AAA-size batteries in parallel (in case one loses charge or is removed), which continuously power the whole MCI for up to 11 h via a 3.3 V linear regulator. BWU circuitry comprises surface-mount components on one side of a two-layer $35 \times 49 \times 1.5$ mm^3 printed circuit board (PCB). A mixed-signal microcontroller (μC; MSP430F1611, Texas Instruments, Dallas, TX, USA), running at 8 MHz, controls the system. Using a second timer running at 32.768 KHz, the μC samples gyroscope in the HWU every 5 ms ($\mathrm{f_s} = 200$ Hz) and controls stimulus pulse timing with ± 30 μs precision. A Bluetooth module (RN-42, Roving Networks, Los Gatos, CA, USA) facilitates parameter changes for patient fitting. This small ($13 \times 26 \times 2$ mm^3) low power device provides wireless communication at up to 3 Mb/s, enabling subjects to move within 20 m of a fitting computer while parameters are adjusted. All components are encased in a plastic housing for protection and easy attachment to the patient's belt. Including batteries, the whole BWU weighs $\sim$49 g.

C. Head-Worn Unit

HWU circuitry occupies both sides of a four-layer $18 \times 15 \times 1.5$ mm^3 PCB including a "slave" μC (MSP430F1611) that receives commands from the BWU via I2C and relays them to the IS via the CI's RF link, a surface-mount tri-axial ITG-3200 gyroscope (InvenSense, Sunnyvale, CA, USA) for angular velocity measurement, and a ADXL345 tri-axial linear accelerometer (Analog Devices, Norwood, MA, USA). The gyroscope that we are using for the MCI is more sensitive than the ones that we used previously with the MVP, at 14 $\mathrm{LSB}/^\circ/\mathrm{s}$ using a 16-bit ADC embedded in the device. As with our previous MVP design, an accelerometer is included in the HWU to accurately measure the HWU's orientation relative to the skull during the fitting sessions [18]. These measurements would in turn allow the real time software to compensate for misalignment between SCC's and the HWU's gyroscope axes.

HWU components are encased in a plastic housing coupled magnetically across the scalp to the IS via three replaceable magnets arranged to align with magnets on the IS, positioning the HWU so that gyroscope axes approximately align with the SCC axes. The HWU weighs $\sim$10 g without magnets and $\sim$18 g with the heaviest magnets.

D. Internal Stimulator

The MCI uses a modified "Concerto" IS (Med-El Elektromedizinische Gerate GmbH, Innsbruck, Austria). Its $25 \times 17 \times 4.5$ mm^3 hermetic housing, inductive coil, 12 feedthroughs and internal circuitry remain unchanged. However, two alterations were made.

The first modification replaces the standard CI electrode array with a new array designed for stimulation of the vestibular nerve. The electrode array design was developed for nonhuman primate studies for use with the MVP [18]. In brief, an array of nine active and two reference 90/10 Pt/Ir electrode contacts is embedded within two silicone carriers. The design is based on anatomic measurements from 3-D reconstructions of macaque temporal bones. A dual fork-shaped array facilitates placement into the horizontal and superior SCC ampullae, while a second array facilitates placement into the posterior SCC ampulla. The reference electrode can be positioned either in the temporalis muscle or in the perilymphatic space of the common crus within the labyrinth.

The second modification is the addition of magnets for enhanced internal-external device coupling. The need for accurate head velocity measurements and continuous stimulation re-

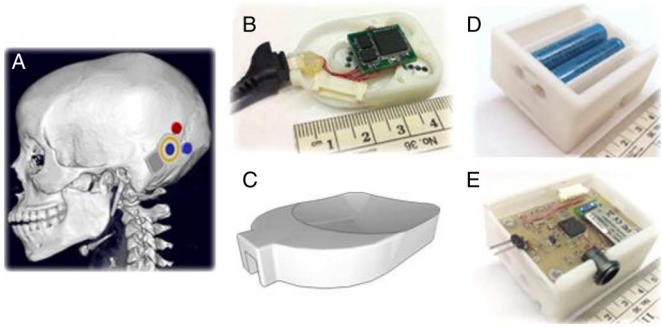

Fig. 2. (a) The IS, which delivers electrical pulses to the vestibular nerve, is shown with supplementary fixation magnets. Its location and position on skull should approximately align gyroscope axes on the HWU with each semicircular canal. (b) Top of HWU (without lid) containing circuitry for 3-D head motion measurement and pulse command relay to the IS. (c) Bottom of HWU, curved at 7.8 cm radius to adapt to the curvature of the average human skull. Images (d) and (e) show the sides of the BWU (without lids) where batteries and circuitry are held, respectively.

quires no slippage or rotation of the HWU relative to the IS. Two implantable medical grade magnets (VORP, Med-El Corp.) were added to the periphery of the Concerto's magnetic coil, in a triangular configuration with an existing central Concerto magnet [Fig. 2(a)]. The polarity of one magnet is reversed to ensure correct placement.

E. Software

Software controlling MCI function is written in C and conveyed to the μCs via a JTAG interface. In the BWU μC, a main program runs continuously in a low power mode with periodic interruptions by one of two timer-driven interrupt service routines (ISRs): 1) a sensor sample (SS) ISR, which samples the gyroscopes at 200 Hz, and 2) a pulse command delivery (PCD) ISR, which sends pulse commands to the HWU μC at the moment when a pulse must be delivered. One pulse command is sent for each stimulation pulse—two 8-bit words specifying the following: The first word specifies the current amplitude (8 bits specifying current between 0 and 700 $\mu\mathrm{A/phase}$). The second word contains the specifications for the stimulation channel (4 bits indicating channel number 1–12) and the pulse width (PW) (2 bits specifying 50, 150, 200, or 300 $\mu\mathrm{s/phase}$), and 2 parity bits.

The SS ISR uses a 16-bit continuous counter driven by a 32.768 KHz sub-main clock (SMCLK) to interrupt the main program every 5 ms and read the digital output from the sensors. Obtaining the three measurement values for each rotation axis from the gyroscope once takes 231 μs. As soon as the values are stored, the BWU μC immediately returns to the main program.

When new gyroscope samples are available, the main program updates stimulation pulse rates by calculating the "time-until-next-pulse" (TUNP) for each channel (taking 180 μs per channel), as described in detail by Chiang *et al.* 2011 [18]. Briefly, angular head velocities obtained from the gyros in $^\circ/\mathrm{s}$ are converted into instantaneous pulse frequencies using a 32-point piecewise-linear approximation to a sigmoid curve, where gyro input ranges from 0 (corresponding to 500°/s head rotation toward the implanted labyrinth) to 4095 (500°/s away), with 2048 corresponding to zero head velocity. A 32 bin look-up table of slopes and intercepts facilitates efficient calculation of this nonlinear mapping function in a compromise between computational time and memory use. After scheduling the pulses the BWU μC enters sleep mode again.

The PCD ISR interrupts the main program whenever a stimulation channel's TUNP timer reaches zero, and sends a pulse command, one 8-bit word at a time with parity checking, to the HWU μC via I2C. Occasionally, the asynchronous PCD routine for a given channel must wait briefly until another channel finishes delivering a pulse command, or until the sensors are sampled, before executing.

F. External Circuitry Housing

Housings were prototyped for both external circuits, as shown in Fig. 2. Designs were developed in SketchUp (Google, Mountain View, CA, USA) and fabricated using a 3-D printer via layered acrylonitrile butadiene styrene plastic deposition. The $45 \times 31 \times 10$ mm^3 HWU housing shown in Fig. 2(b) and (c) accommodates circuitry, an RF coil and three medical grade magnets chosen to accommodate the user's scalp thickness. Magnets are angled inward to fit the radius of curvature of the average adult human skull's scalp near the asterion -7.8 ± 0.7 cm, measured using a dataset of human head CAT scans (unpublished data). A CAD drawing of the outer aspect of the HWU is shown in Fig. 2(c) to emphasize the curvature of the device, which is otherwise difficult to observe in a photograph. This side of the HWU's housing is coated with silicone (A-103 Elastomer, Factor II Inc., Lakeside, AZ, USA) to increase friction. A $53 \times 47 \times 27$ mm^3 protective housing was similarly designed and manufactured to encase the BWU battery pack and circuitry [Fig. 2(d) and (e)].

III. Materials and Methods

A. External System Performance Tests

1) Gyroscope Modulation: Bench-top performance tests were completed to assess the external component's ability to sense head angular velocity and modulate pulse rate. Pulse command signals were observed simultaneously on all channel outputs from the HWU as it rotated sinusoidally on a servo-controlled earth-vertical-axis rotator at 1 Hz with 50°/s peak velocity about the roll, pitch, and yaw axes. Then to test communication reliability, pulse command transmission and reception between BWU and HWU were tested continuously for 24 h at 400 commands/s over a 98 cm cable. The cable was positioned adjacent to unrelated CI head-worn components placed on the test bench to generate RF noise. Since one command is sent for each pulse delivered, we monitored the command and stimulus pulse rates to test for transmission errors. Odd parity bit checking implemented in the software code for the master (BWU) and slave (HWU) microcontrollers was used to detect any error in transmission. Parity bits in the data sent and data received were compared, and a counter was used to keep track of the number of bit flips during data transmission/reception.

We also tested for possible effects of the magnets on the vestibular prosthesis' ability to detect motion. The HWU, containing the gyroscopes, was mounted on the servo-controlled

earth-vertical-axis rotator. Frequency modulated pulse command signals were monitored on an output channel as the HWU was rotated sinusoidally at 1 Hz with ±50 dps peak velocity about the pitch axis. The pulse rates were compared for 10 cycles of each of the following cases: HWU in the presence of no magnets, one, and three (in a triangular configuration) Amade five magnets (the strongest magnets used in our force/pressure measurements).

2) Magnetic Retention Forces and Pressure: Proper MCI function requires the HWU to remain securely coupled to the IS across the scalp to both transduce head motion accurately and maintain power and signal transmission. (Abrupt HWU-IS decoupling would halt stimulation, causing vertigo and nystagmus due to a sudden drop in vestibular nerve activity. Relative motion between the HWU and IS would cause less severe but nonetheless unpleasant symptoms due to inaccurate perception of head motion and misalignment between head motion and reflexive responses of extraocular and postural muscles.) While fixation could be accomplished using percutaneous posts implanted in the skull, that approach allows a path around the post for transit of infection. We, therefore, sought to determine whether coupling could be achieved using high-field rare-earth medical grade magnets such that retention forces are sufficient to maintain coupling during daily activities without preventing capillary perfusion.

Threshold decoupling forces were measured across the scalp of a human cadaver temporal bone (TB) specimen and the pressure exerted on the scalp was calculated. Tissue thickness was measured at each magnet site. A post-auricular incision was made, the modified IS was implanted, and the incision was sutured closed. The HWU was then magnetically attached across the scalp, and threshold decoupling forces were measured by pulling in the superior, anterior, inferior, and outward directions with a digital hanging scale (SR-1 1000 g × 1 g, American Weigh Scales Inc., Norcross, GA, USA). Superior, anterior and inferior refer to the directions with respect to the skull in standard erect anatomic orientation; "outward" denotes a direction perpendicular to the surface of the skull. Five measurements were made in each direction using each of six combinations of different magnets—MedEl Amade #3, #4, and #5, with residual flux densities of 1.17, 1.33, and 1.39 T, respectively. The strongest magnet was always placed in the center position (Fig. 2).

Lack of TB specimens uniformly spanning the range of typical human adult scalp thicknesses (90/10—percentile is from 3.5–8 mm [19]) prompted us to use a synthetic material to simulate scalp tissue in subsequent measurements. Preliminary investigation showed the texture and consistency of cork would provide an adequate approximation to scalp tissue. Thin cork pads were stacked and attached to a plastic human skull model, and force and pressure measurements were obtained in the same manner as with the TB specimen.

B. Internal System Performance Tests

To verify functionality of the internal system, we used the Pulsar IS (Med-El), a ceramic encased IS that functions in the same way as the Concerto IS (which replaced the Pulsar in later design iterations). The Pulsar IS was controlled via a

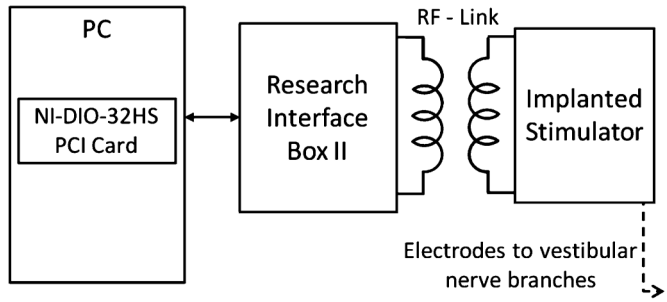

Fig. 3. Setup used to test performance of the internal system. A computer sinusoidally modulated virtual head rotations and calculated timing of pulse commands, which were sent to the implanted stimulator via the research interface box's (RIBII) inductive link. Frequency-modulated biphasic charge-balanced pulses were delivered to each of the monkey's semicircular canals.

Research Interface Box II (RIB II; Leopold-Franzens-University of Innsbruck, Austria [20]) (Fig. 3). We used this separate setup to test the internal system performance due to proprietary restrictions on the RF design associated with the Med-El hardware.

1) Current Amplitude Measurements: Prior to animal testing, the current delivered by the Pulsar and by our lab-built MVP2 were measured on a test-bench using a sense resistor wired in series with a Teflon-coated steel wire (Cooner Wire, Chatsworth, CA, USA) submerged in 0.9% NaCl saline.

2) In vivo Physiological Studies: Studies were performed on two rhesus monkeys (F20124RhB and F060738RhG, referred to as monkey A and monkey B respectively; Macaca mulatta; 5–12 kg) under a protocol approved by the Johns Hopkins Animal Care and Use Committee, which is accredited by the Association for the Assessment and Accreditation of Laboratory Animal Care, and consistent with European Community Directive 86/609/EEC. The purpose of these experiments was to test if the MCI can deliver stimulation pulse trains evoking responses similar to those elicited with the MVP2.

a) Surgery: Each animal was implanted with 1) an acrylic head cap surgically affixed to the skull to aid in stereotaxic placement during experiments, 2) two scleral coils for 3-D measurement of eye movements, and 3) an array of electrodes inserted into the left ampullae. Vestibular function was ablated via intratympanic injection of gentamicin. Procedures were performed under sterile conditions and 1.5%–5% isoflurane anesthesia.

Surgical methods of head-cap, scleral coil, and electrode implantation have been previously described [18], [21]–[23]. In brief, a light poly-ether-ether-ketone head cap was first affixed to the animal's skull using titanium bone screws. Then, two polytetrafluoro-ethylene-coated steel wire (Cooner Wire, Chatsworth, CA, USA) search coils were sutured to the sclera of each eye—one around the iris and another roughly orthogonal to the first-, and wires were run to the connectors within the head cap. In a separate surgical session, electrodes were implanted into the left labyrinth. First, a mastoidectomy was performed, followed by exposure of the SCCs, each of which was then opened near the junction of the thin segment and the ampulla. The forked electrode array was inserted near the junction of the superior and horizontal SCCs, and the single-tine

array was inserted into the posterior SCC. Additional reference electrodes were inserted in the labyrinth and beneath the temporalis muscle [21], [24]. Electrode leads were then run under periosteum and terminated in a connector on the head cap so our MVP2 or MCI connector could be attached.

After recovery from implantation, intratympanic gentamicin was administered using a standard clinical dosing regimen similar to the one used in humans [25]. During each treatment, $\sim$0.5 mL of 26.7 mg/mL buffered gentamicin solution was injected through the ear drum into the middle ear, resulting in ablation of labyrinthine mechano-sensitivity. Treatments were repeated every three weeks until vestibulo-ocular reflex (VOR) responses to ipsilateral head rotations had $<$10% of normal gain. In each case, 2–3 injections per ear were required.

b) Stimulation paradigm: VOR responses were elicited using the Pulsar and our MVP2 to present frequency-modulated, charge-balanced, cathodic-first (at the SCC electrode), 150 μs per phase, biphasic pulse stimuli, similar to those used in our previous primate experiments with the dedicated MVP2 [26]. To ensure evoked responses were due solely to prosthetic stimulation, animals were kept stationary (no head or body rotation/translation) and gyroscope signals were replaced with software controlled digital signals representing virtual head rotations. Stimulation pulse timing was calculated by a computer, which passed pulse command signals determining pulse timing, PW, current amplitude and active electrode to the Pulsar via the RIB II's RF link.

Before starting each experiment, electrode currents were optimized by defining thresholds and maximal levels at which signs of current spread occur, and setting constant amplitudes to 10% below the maximum level. Current was slowly increased while sinusoidal pulse rate modulation corresponding to virtual 1 Hz, 50°/s head movement was delivered to the electrodes (see the mapping between head velocity and pulse rate description below). Threshold current was determined to be the current amplitude at which eye movements of $\sim 10^\circ/\mathrm{s}$ were observed, and maximum current was determined to be just below the current that elicited large eye movement axis changes ($\geq 30^\circ$ axis shift visible to an examiner viewing an infrared video feed of the eyes) or visible facial muscle responses (both indicating unacceptable current spread). Stimulation thresholds vary between SCCs and between animals, so different current amplitudes were used for each SCC, ranging from 100–200 μA.

Once currents were optimized, the animal was stimulated at the 96 pulses-per-second (pps) baseline rate until the frequency of nystagmus—fast reflexive eye movements due to asymmetric input from the two vestibular labyrinths—fell to $<$1 per 30 s of observation. This took $\sim$5 min. Then, stimuli based on a previously described velocity-to-frequency map designed to emulate normal behavior of rhesus vestibular primary afferents ($f_{base} = 96$ pps, $f_{max} = 350$ pps, $C = 2$; based on [27]) were delivered, modulated by virtual sinusoidal head rotations at 0.1, 0.2, 0.5, 1, 2, and 5 Hz with 50, 100, and 200°/s peak velocities. This set of 18 different stimulus pulse patterns was presented to each SCC with the animal in complete darkness to ensure the VOR was not suppressed by visual input. Modulated stimuli were given to one SCC at a time (while stimulating the other two at a constant baseline rate), first with the MVP2 and then with the MCI. Each stimulus pulse pattern was given for 10–20 sinusoidal cycles, depending on the stimulus frequency, returning to baseline stimulation for 5 s between each set. An LED placed directly in front of the monkey's face was flashed to re-center gaze before each pulse pattern.

C. Eye Movement Recording

Our custom-built system used to measure 3-D angular eye position has been previously described in detail [21]. In short, the monkey was seated in a plastic chair restrained by the skull cap and secured to the rotator. Three pairs of field coils were attached to the superstructure, generating three fields orthogonal to each other and aligned with the X (nasooccipital, +nasal), Y (interaural, +left), and Z (superoinferior, +superior) head coordinate axes. The X, Y, and Z field signals induced across each scleral coil were demodulated, filtered, and analyzed using 3-D rotational kinematic methods [23], [28]. Angular rotations were expressed as rotation vectors with roll, pitch, and yaw coordinates, and angular velocity vectors of eye with respect to head were calculated from the corresponding rotation vectors [29]–[31].

D. Eye Movement Analysis

Eye movement data analysis methods have been previously described in detail [7]. Briefly, data were analyzed using a custom software package written in LabVIEW that incorporates 3-D rotational kinematics [32]. The eye movements were calculated in the reference frame corresponding to the SCC axes: the left-anterior/right-posterior axis (LARP), the right-anterior/left-posterior axis (RALP), and the horizontal axis. 3-D Eye rotation velocity was calculated from linearly interpolated and filtered eye movement data. Peak eye velocity was calculated for each cycle-averaged pulse train. Trials in which the monkey blinked or fell asleep were disregarded. Aggregate values are reported as mean $\pm$ sample standard deviation.

IV. Results

A. External System Performance

1) Gyroscope Modulation: Instantaneous pulse frequency traces from each output channel (Fig. 4) confirm the external system's ability to modulate pulse rate based on real-time sensor input. During yaw rotations, only pulse rate on the horizontal (z) channel modulated. Pitch rotations elicited anti-phase modulation of the LARP and RALP channels, while roll rotations elicited in-phase modulation.

No errors indicated by bit flips were detected in the course of continuous pulse command transmission and reception between the BWU and HWU over 24 h at a rate of 400 commands/s. We conclude that cable length and close proximity to active RF hardware does not affect I2C communication.

To test the possible effects of the presence of magnets on detecting head movement with the HWU, we rotated the HWU in the presence of no magnets, one magnet, and three magnets. The maximum and minimum pulse rates reached 126.7 $\pm$ 0.47 pps and 62.3 $\pm$ 0.46 pps with no magnets, 126.8 $\pm$ 0.62 pps and 62.0 $\pm$ 1.44 pps with one magnet, and 127.1 $\pm$ 0.73 pps

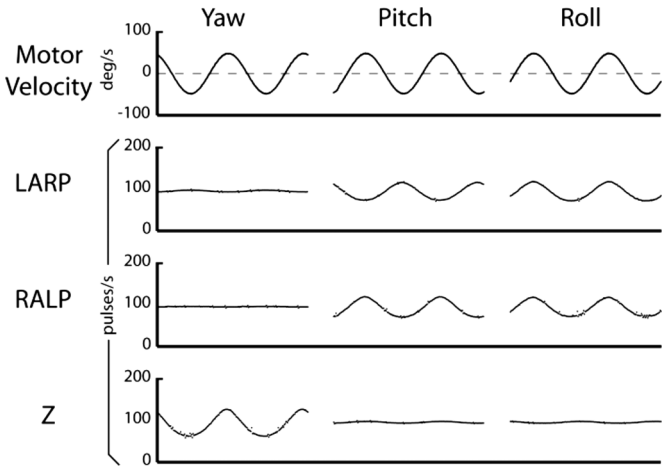

Fig. 4. Time plots of real-time pulse-command rate modulation by the modified cochlear implant's external system in response to on-axis sinusoidal yaw, pitch, and roll rotations, at 1 Hz with a peak velocity of $\pm 50^\circ/\mathrm{s}$. Recordings were taken on three channels concurrently. Occasional pulse rate irregularities occurred due to a timing error that arose at certain stimulator pulse rates. That error was discovered and fixed after completion of the physiological studies presented in Figs. 6 and 7.

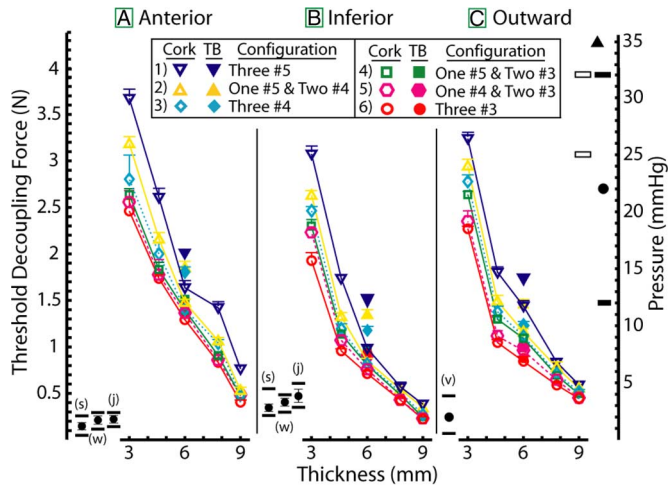

Fig. 5. HWU was attached to the IS using various magnet combinations across different tissue thicknesses and pulled in the (a) anterior, (b) inferior, and (c) outward directions. Filled and empty shapes denote measurements taken using TB and cork pads, respectively. Filled circles on left of each plot denote forces on the head during walking (w), jogging (j), climbing stairs (s), and voluntary yaw rotations (v); rectangles denote minimum and maximum. Pressure exerted by all magnet combinations is indicated on the axis at the right of the figure. Mean, arteriolar, and venous end pressures according to Landis [1] are denoted by the circle and filled rectangles. Capillary pressure ranges according to Steinmetz and Langemo [2] are denoted by the empty rectangles. Occipital capillary pressure according to Ryan *et al.* [3] is denoted by the filled triangle.

and 62.4 $\pm$ 1.2 pps with three magnets. The modulation cycle periods were 1.0 $\pm$ 0.0045 s with no magnets, 1.0 $\pm$ 0.0044 s with one magnet, and 1.0 $\pm$ 0.0046 s with three magnets. The maximum pulse rate difference between the no-magnet condition and either the one or the three magnet conditions was 0.24% (or 0.23 pps). We did not observe any qualitative difference between the pulse rate trajectories when the magnets were present and when they were not. We conclude that the accuracy of the HWU measurement of head rotation is not degraded by the presence of magnets.

2) Magnetic Retention Forces and Pressure: Fig. 5 shows force measurements taken using various combinations of external magnets. During routine daily activities, based on the maximum HWU weight of 17.56 g, the HWU would experience the greatest anterior/tangential and inferior/tangential forces (222 $\pm$ 40 and 474 $\pm$ 71 mN, respectively) while jogging (j) and the greatest outward/centrifugal force (3 $\pm$ 2 mN) while climbing down stairs (s). In extreme cases, vigorous voluntary yaw rotations (v) can reach average peak velocities of $\sim 780^\circ/\mathrm{s}$ (ranging from 380–1100$^\circ/\mathrm{s}$) [33] and the HWU can experience average outward/centrifugal forces of $\sim$253 mN. However, such high velocities are not reached during routine head movements. It is worth noting that outward forces due to walking, jogging, and climbing stairs are $\leq$1.2% of the force experienced during voluntary yaw rotations and they are too small to be seen in Fig. 5(c). In the anterior and outward directions [Fig. 5(a) and (c)] decoupling thresholds with all magnet combinations across all tissue thicknesses were greater than or equal to the maximum anterior and outward forces expected for the HWU during jogging in Fig. 5(a), and vigorous voluntary yaw rotations in Fig. 5(c). In the inferior direction [Fig. 5(b)], not all magnet combinations provided sufficient retention force across all tissue thicknesses. For 6 mm and thinner tissue, decoupling thresholds for all combinations were $\geq$150.3% of the mean jogging decoupling forces. For 7.8 mm tissue, however, combinations 1–4 were marginal at $\geq$101%, while combinations 5 and 6 yielded $\leq$92% of the forces, meaning that the HWU could fall off in those circumstances. Similarly, for 9 mm tissue, all thresholds were $\leq$81% of the mean jogging decoupling forces.

Fig. 5(c) (right side axis) shows pressure exerted by HWU-IS coupling on the intervening tissue using different magnet combinations. No single definitive capillary blood pressure value was found in literature and the measurements presented by multiple sources are shown in the plot. Here we use the most commonly accepted mean capillary pressure (MCP) measurements reported by Landis (indicated with a black dot along the right axis, $\mathrm{MCP} = 22\ \mathrm{mmHg}$) [1] as our benchmark criteria. For scalp thickness $\geq$4.7 mm, pressure exerted by all magnet combinations was below the MCP. For 3 mm, magnet combinations 1, 2, and 3 exceeded the MCP at 120%, 110%, and 103% of MCP respectively, and combinations 4–6 were below the MCP at $\leq$98% of MCP.

B. Internal System Performance

1) Current Measurements: Current delivered by each channel was quantified for both the Pulsar and the MVP2. In most cases, actual current delivered was slightly different than expected, yet never below 93% of the expected value. As determined by the area under the biphasic curves, the MCI delivered 99.3% of the charge delivered by the MVP2.

2) In Vivo Physiological Experiments: Fig. 6 shows a side-by-side comparison of responses elicited by both prostheses in monkey A, for one cycle of sinusoidal pulse frequency modulated stimulation of each SCC at 1 Hz from 68–130 pps (equivalent to 50$^\circ/\mathrm{s}$ peak velocity in normal animals using the previously referenced velocity-to-frequency sigmoidal map). Standard deviation was less than 3.8$^\circ/\mathrm{s}$ for all traces. Fig. 7

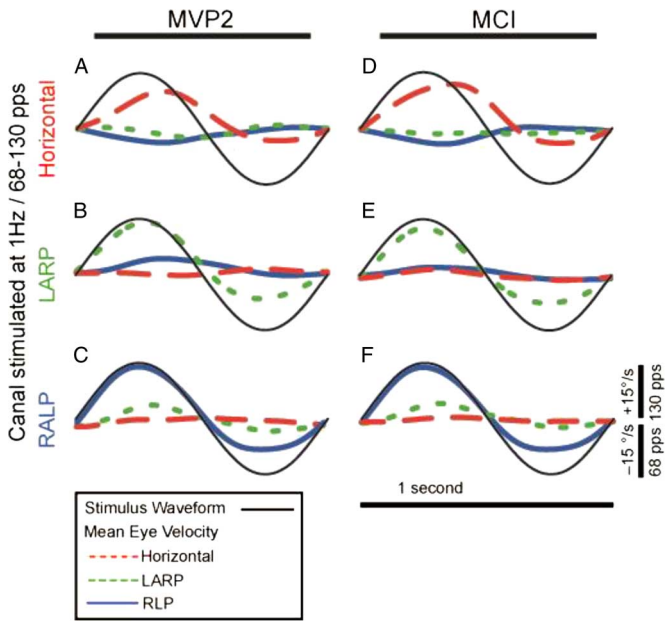

Fig. 6. Comparison of 3-D vestibulo-ocular reflex peak responses elicited in rhesus monkey A by delivering stimulation pulses to each canal using our lab-built MVP2 (A–C) and the Pulsar IS (D–F). Stimulus was sinusoidally modulated at 1 Hz from 68–130 pps peak (corresponding $\pm 50°/s$ in a normal animal). Standard deviation was $\leq 3.8°/s$ for all traces.

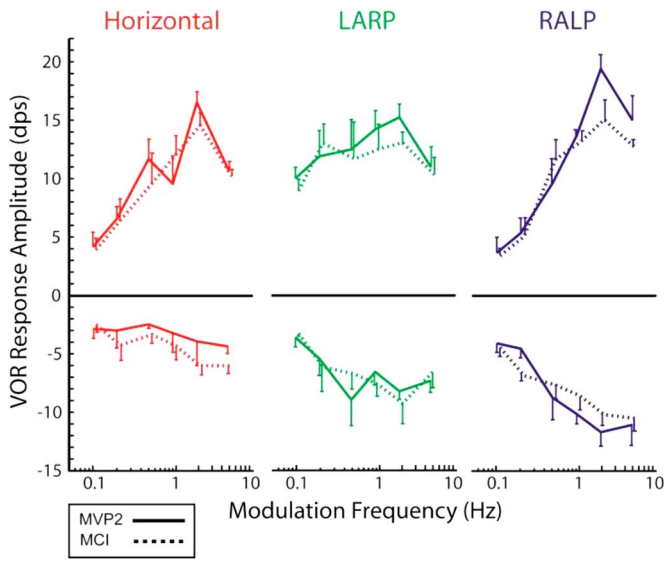

Fig. 7. Excitatory and inhibitory 3-D vestibulo-ocular reflex responses elicited in rhesus monkey "A" by stimulating each left canal using our lab-built MVP2 (solid line) and the MCI (dotted line). Stimulus was modulated at 1–5 Hz from 68–130 pps peak (equivalent to $\pm 50°/s$ in a normal animal), using the head-velocity to pulse rate mapping curve with $C = 2$, baseline pulse rate 96 pps, maximum pulse rate 350 pps, and current at 150, 170, 200 uA for the horizontal, left-anterior, and left-posterior canals, respectively. Mean responses ranged from 2.9–16.5°/s with the MVP2 and from 2.5–14.6°/s with the MCI.

shows excitatory and inhibitory amplitude responses elicited in monkey A with both prostheses. Difference in responses evoked with each prosthesis were $\leq 4.3°/s$ for monkey A and $\leq 4.7°/s$ for monkey B across all stimulation frequencies (0.1–5 Hz), for all sinusoidally modulated stimuli. Combining data for both monkeys, MVP2 responses ranged from 2.6–20.1°/s and MCI responses ranged from 2.2–19.8°/s.

V. Discussion

To expedite realization of a vestibular prosthesis for clinical use, we sought to replace the external components, control software and electrode array of a commercially available CI system and to determine whether it could function as an MVP. While we could not conduct the final tests of the complete MCI system due to proprietary constraints associated with the RF link between the HWU and the IS, we successfully tested both the external (HWU and BWU) and the implanted (IS) parts of the overall system. Although definitive assessment shall require a clinical trial employing a fully integrated MCI system, our results indicate that the MCI approach is a promising alternative for implementation of a vestibular prosthesis to restore balance sensation.

Size and power: Uninterrupted stimulation and accurate head motion measurement are important for proper function of an MVP, so the HWU must be as small and light as possible to reduce the possibility of accidental decoupling or slippage. HWU size and weight have been minimized by placing components that do not require head fixation or proximity to the IS in the BWU. The inductive power link avoids the need for a percutaneous connection and reduces risk of infection, but it incurs poorer power transmission efficiency. The BWU allows use of a large battery pack to supply the high current demands, and it includes a backup battery to maintain continuous function when a battery must be replaced.

Gyro modulation tests: As expected, slight stimulus asymmetry in pulse rate curves (Fig. 4) is seen for pulse rate above versus below the 96°/s baseline. This asymmetry is the result of the nonlinear sigmoidal relationship between the gyroscope measurements and the corresponding pulse rates computed in the BWU μC.

Magnetic retention forces and pressure: Although an extensive literature search did not identify a single consensus value for a "safe threshold" external pressure below which scalp perfusion is not compromised, available literature suggests that it is likely to be somewhere in the range of 20–25 mmHg. Arteriolar- and venous-end capillary perfusion pressures provide liberal and conservative extremes, but the mean capillary perfusion pressure (e.g., 22 mmHg per the Landis study), seems to have become the consensus criterion for scenarios like the MVP.

Optimal coupling can be achieved using different magnet combinations for scalp tissue ranging from 4.6–7.8 mm. For patients with scalp >7.8 mm, retention force would not be sufficient to maintain stable coupling through the range of active head movements. Because the coupling pressure was significantly below the MCP for these patients, it would be possible to add extra magnets to establish a more secure coupling without incurring the extra safety risk. For patients with scalp <4.6 mm, pressure exerted on the tissue would exceed the MCP for magnet combinations 1, 2, and 3. Because the magnet pressure appears to be only marginally below the MCP for the magnet combinations 4, 5, and 6, magnet strength can be reduced further by placing other nonferromagnetic material under each magnet in the HWU housing.

The difference between the measurements taken using cork and the TB specimen increased as magnetic force increased. On the TB specimen more force was required to decouple the

HWU likely due to the higher compressibility of the scalp which allows the HWU to slightly dimple the tissue and resist greater tangential forces. All measurements taken with the human TB specimen with scalp tissue ∼6 mm are well fit to the regression lines defined by the cork data, being ≤532 mN away from the regression line in each case.

One could convert the force data we report into torques by arbitrarily specifying a center of rotation. We elected not to do that because no single center of rotation sufficiently dominates the rotational motion experienced in activities of daily living. (One could choose the center of the head, but data would still have to be rescaled by the moment arm for rotation about any other point.)

In vivo stimulation: Data in Figs. 6 and 7 show that the MCI's implantable stimulator evokes responses in rhesus monkeys comparable to those evoked with the MVP2 to partially restore the 3-D VOR for head rotations about each SCC axis. However, some nonidealities were seen.

First, LP canal stimulation yielded responses of greater magnitude than the LA or LH canals. This could be due to the LP electrode being closer to its target than other electrodes were to theirs.

Second, an excitatory versus inhibitory asymmetry was seen in the eye responses in Figs. 6 and 7. Asymmetry is an inherent feature of VOR responses driven by a single normal ear [34]. It is more apparent during prosthetic stimulation because pulsatile stimuli cannot depress vestibular nerve primary afferent fibers' firing rates below their spontaneous discharge rates. Stimulation protocols in which subjects are allowed to adapt to supernormal baseline rates during pulse frequency and amplitude "co-modulation" are effective in reducing asymmetry [35]. While we did not explicitly test this stimulation strategy the MCI is fully capable of implementing this protocol.

Lastly, although responses were greater in the plane of the stimulated SCC, spurious stimulation of nontarget nerves results in misalignment (i.e., eye movements do not precisely align with the 3-D axis of head rotation). This is likely due to current spread. We previously showed that incorporating a pre-compensatory 3-D coordinate transformation in the prosthesis can reduce the misalignment [9]. Although the MCI's HWU incorporates a microcontroller similar to the one that implements this coordinate transformation protocol in the MVP2, we have not yet implemented that protocol in the MCI.

Future directions: We tested external and internal systems separately and verified their functionality. Efforts to combine both systems into one complete, fully functional MCI are underway. Once this is accomplished, we intend to replicate results obtained with our previous MVPs, implementing novel stimulation protocols and algorithms recently developed by our lab to elicit more symmetric responses and improve misalignment [9], [35]. Results to date suggest that realization of the first human-implantable MVP for treatment of BVH is possible using this approach.

ACKNOWLEDGMENT

The authors gratefully acknowledge contributions of A. Jäger, R. Hessler, and A. Hofner (Med-El Elektromedizinische Gerate GmbH; modified Concerto CI and associated hardware); E. Hochmair and O. Peter (University of Innsbruck; RIBII); N. Davidovics, M. Rahman, B. Chiang, B. Ward, J. Ho Ahn, and L. Swarthout (Johns Hopkins; analysis software, MVP2 fabrication, editing, and animal care). C. Della Santina holds an equity interest in and is CEO of Labyrinth Devices, LLC, a start-up company founded to support commercialization of vestibular prosthesis technology. Terms of this arrangement are managed by the Johns Hopkins University in accordance with its conflict of interest policies.

REFERENCES

[1] E. Landis, "Micro-injection studies of capillary blood pressure in human skin," *Heart*, vol. 15, 1930.

[2] J. A. Steinmetz and D. K. Langemo, "Changes in occipital capillary perfusion pressures during coronary artery bypass graft surgery," *Adv. Wound Care*, vol. 9, no. 3, pp. 28–32, May–Jun. 1996.

[3] D. Ryan, V. Allen, and A. Murray, "An investigation of interface pressures in low air loss beds," *Int. J. Clin. Pract.*, vol. 51, no. 5, pp. 296–298, 1997.

[4] C. C. Della Santina, A. A. Migliaccio, R. Hayden, T. A. Melvin, G. Y. Fridman, B. Chiang, N. S. Davidovics, C. Dai, J. P. Carey, L. B. Minor, I. C. Anderson, H. Park, S. Lyford-Pike, and S. Tang, "Current and future management of bilateral loss of vestibular sensation—An update on the Johns Hopkins multichannel vestibular prosthesis project," *Cochlear Implants Int.*, vol. 11, no. Suppl 2, pp. 2–11, Sep. 2010.

[5] M. A. Rahman, C. Dai, G. Y. Fridman, N. S. Davidovics, B. Chiang, J. Ahn, R. Hayden, T. A. Melvin, D. Q. Sun, A. Hedjoudje, and C. C. Della Santina, "Restoring the 3-D vestibulo-ocular reflex via electrical stimulation: The Johns Hopkins multichannel vestibular prosthesis project," in *Proc. IEEE Eng. Med. Biol. Soc. Conf.*, 2011, vol. 2011, pp. 3142–3145.

[6] C. Dai, G. Y. Fridman, B. Chiang, N. S. Davidovics, T. A. Melvin, K. E. Cullen, and C. C. Della Santina, "Cross-axis adaptation improves 3-D vestibulo-ocular reflex alignment during chronic stimulation via a head-mounted multichannel vestibular prosthesis," *Exp. Brain Res.*, vol. 210, no. 3–4, pp. 595–606, May 2011.

[7] N. S. Davidovics, G. Y. Fridman, B. Chiang, and C. C. Della Santina, "Effects of biphasic current pulse frequency, amplitude, duration, interphase gap on eye movement responses to prosthetic electrical stimulation of the vestibular nerve," *IEEE Trans. Neural Syst. Rehabil. Eng.*, vol. 19, no. 1, pp. 84–94, Feb. 2011.

[8] D. Q. Sun, M. A. Rahman, G. Fridman, C. Dai, B. Chiang, and C. C. Della Santina, "Chronic stimulation of the semicircular canals using a multichannel vestibular prosthesis: Effects on locomotion and angular vestibulo-ocular reflex in chinchillas," in *Proc IEEE Eng. Med. Biol. Soc. Conf.*, 2011, vol. 2011, pp. 3519–3523.

[9] G. Y. Fridman, N. S. Davidovics, C. Dai, A. A. Migliaccio, and C. C. Della Santina, "Vestibulo-ocular reflex responses to a multichannel vestibular prosthesis incorporating a 3-D coordinate transformation for correction of misalignment," *J. Assoc. Res. Otolaryngol.*, vol. 11, no. 3, pp. 367–381, Sep. 2010.

[10] W. Gong and D. M. Merfeld, "Prototype neural semicircular canal prosthesis using patterned electrical stimulation," *Ann. Biomed. Eng.*, vol. 28, no. 5, pp. 572–581, May 2000.

[11] C. C. Della Santina, A. A. Migliaccio, and A. H. Patel, "A multichannel semicircular canal neural prosthesis using electrical stimulation to restore 3-d vestibular sensation," *IEEE Trans. Biomed. Eng.*, vol. 54, no. 6, pp. 1016–1030, Jun. 2007.

[12] C. Della Santina, A. Migliaccio, and A. Patel, "Electrical stimulation to restore vestibular function development of a 3-d vestibular prosthesis," in *Proc. IEEE Eng. Med. Biol. Soc. Conf.*, 2005, vol. 7, pp. 7380–7385.

[13] C. Wall, M. I. Kos, and J. P. Guyot, "Eye movements in response to electric stimulation of the human posterior ampullary nerve," *Ann. Otol. Rhinol. Laryngol.*, vol. 116, no. 5, pp. 369–374, May 2007.

[14] J. T. Rubinstein, J. Phillips, K. Nai, L. Ling, S. Bierer, E. Jameson, and T. Oxford, "Clinical, scientific, regulatory roadmap for a human vestibular implant," presented at the ARO 2011 Midwinter Meet., Baltimore, MD.

[15] J. P. Guyot, A. Sigrist, M. Pelizzone, and M. I. Kos, "Adaptation to steady-state electrical stimulation of the vestibular system in humans," *Ann. Otol. Rhinol. Laryngol.*, vol. 120, no. 3, pp. 143–149, Mar. 2011.
[16] J. P. Guyot, A. Sigrist, M. Pelizzone, G. C. Feigl, and M. I. Kos, "Eye movements in response to electrical stimulation of the lateral and superior ampullary nerves," *Ann. Otol. Rhinol. Laryngol.*, vol. 120, no. 2, pp. 81–87, Feb. 2011.
[17] D. Lasker and M. Schubert, "3-D measurement of linear accelerations and angular velocities of the head, torso and leg during natural activities," presented at the ARO 35th Annu. Midwinter Res. Meet., San Diego, CA, 2012.
[18] B. Chiang, G. Y. Fridman, C. Dai, M. A. Rahman, and C. C. Della Santina, "Design and performance of a multichannel vestibular prosthesis that restores semicircular canal sensation in rhesus monkey," *IEEE Trans. Neural Syst. Rehabil. Eng.*, vol. 19, no. 5, pp. 588–598, Oct. 2011.
[19] C. H. Raine, C. A. Lee, D. R. Strachan, C. T. Totten, and S. Khan, "Skin flap thickness in cochlear implant patients—A prospective study," *Cochlear Implants Int.*, vol. 8, no. 3, pp. 148–157, Sep. 2007.
[20] A. Bahmer, O. Peter, and U. Baumann, "Recording and analysis of electrically evoked compound action potentials (ECAPs) with MED-EL cochlear implants and different artifact reduction strategies in Matlab," *J. Neurosci. Methods*, vol. 191, no. 1, pp. 66–74, Aug. 2010.
[21] A. A. Migliaccio, M. C. Schubert, P. Jiradejvong, D. M. Lasker, R. A. Clendaniel, and L. B. Minor, "The three-dimensional vestibulo-ocular reflex evoked by high-acceleration rotations in the squirrel monkey," *Exp. Brain Res.*, vol. 159, no. 4, pp. 433–446, Dec. 2004.
[22] R. A. Clendaniel, D. M. Lasker, and L. B. Minor, "Horizontal vestibuloocular reflex evoked by high-acceleration rotations in the squirrel monkey. IV. Responses after spectacle-induced adaptation," *J. Neurophysiol.*, vol. 86, no. 4, pp. 1594–1611, Oct. 2001.
[23] D. A. Robinson, "A method of measuring eye movement using a scleral search coil in a magnetic field," *IEEE Trans. Biomed. Eng.*, vol. 10, pp. 137–145, Oct. 1963.
[24] C. Dai, G. Y. Fridman, and C. C. Della Santina, "Effects of vestibular prosthesis electrode implantation and stimulation on hearing in rhesus monkeys," *Hear. Res.*, vol. 277, no. 1–2, pp. 204–210, Jul. 2011.
[25] L. B. Minor, "Intratympanic gentamicin for control of vertigo in Meniere's disease: Vestibular signs that specify completion of therapy," *Am. J. Otol.*, vol. 20, no. 2, pp. 209–219, Mar. 1999.
[26] C. Dai, G. Y. Fridman, N. S. Davidovics, B. Chiang, J. H. Ahn, and C. C. Della Santina, "Restoration of 3-D vestibular sensation in rhesus monkeys using a multichannel vestibular prosthesis," *Hear. Res.*, vol. 281, no. 1–2, pp. 74–83, Nov. 2011.
[27] S. G. Sadeghi, L. B. Minor, and K. E. Cullen, "Dynamics of the horizontal vestibuloocular reflex after unilateral labyrinthectomy: Response to high frequency, high acceleration, high velocity rotations," *Exp. Brain Res.*, vol. 175, no. 3, pp. 471–484, Nov. 2006.
[28] D. Straumann, "The validity of oculomotor laws," *Schweiz Arch. Neurol. Psychiatr.*, vol. 146, no. 4, pp. 151–156, 1995.
[29] T. Haslwanter, "Mathematics of three-dimensional eye rotations," *Vision Res*, vol. 35, no. 12, pp. 1727–1739, Jun. 1995.
[30] A. A. Migliaccio and M. J. Todd, "Real-time rotation vectors," *Australas Phys. Eng. Sci. Med.*, vol. 22, no. 2, pp. 73–80, Jun. 1999.
[31] K. Hepp, "On Listing's law," *Commun. Math. Phys.*, vol. 132, pp. 285–295, 1990.
[32] A. A. Migliaccio, C. C. Della Santina, J. P. Carey, J. K. Niparko, and L. B. Minor, "The vestibulo-ocular reflex response to head impulses rarely decreases after cochlear implantation," *Otol. Neurotol.*, vol. 26, no. 4, pp. 655–660, Jul. 2005.
[33] G. E. Grossman, R. J. Leigh, L. A. Abel, D. J. Lanska, and S. E. Thurston, "Frequency and velocity of rotational head perturbations during locomotion," *Exp. Brain Res.*, vol. 70, no. 3, pp. 470–476, 1988.
[34] J. R. Ewald, *Physiologische Untersuchungen uber das Endorgan desNervus Octavus*. Wiesbaden, Germany: Nabu, 1892.
[35] N. S. Davidovics, G. Y. Fridman, and C. C. Della Santina, "Co-modulation of stimulus rate and current from elevated baselines expands head motion encoding range of the vestibular prosthesis," *Exp. Brain Res.*, vol. 218, no. 3, pp. 389–400, May 2012.
[36] C. Garnham, M. Zimmerling, and A. Jäger, "Vestibular implant system with internal and external motion sensors," U.S. Patent 0 022 616 A1, 2012.
[37] J. O. Phillips, S. J. Shepherd, A. L. Nowack, L. Ling, S. M. Bierer, C. R. S. Kaneko, C. M. T. Phillips, K. Nie, and J. T. Rubinstein, "Longitudinal performance of a vestibular prosthesis as assessed by electrically evoked compound action potential recording," in *Proc. Annu. Int. Conf. IEEE Eng. Med. Biol. Soc.*, 2012, pp. 6128–6131.
[38] K. Nie, L. Ling, S. Bierer, C. Kaneko, A. Fuchs, T. Oxford, J. Rubinstein, and J. Phillips, "An experimental vestibular neural prosthesis: Design and preliminary results with rhesus monkeys stimulated with modulated pulses," *IEEE Trans. Biomed. Eng.*, vol. 60, no. 6, pp. 1685–1692, Jun. 2013.
[39] T. G. Constandinou, J. Georgiou, and C. Toumazou, "A partial-current-steering biphasic stimulation driver for vestibular prostheses," *IEEE Trans. Biomed. Circuits Syst.*, vol. 2, no. 2, pp. 106–113, Jun. 2008.
[40] J. Dai, A. Demosthenous, T. Perkins, X. Liu, and N. Donaldson, "A stimulator ASIC featuring versatile management for vestibular prostheses," *IEEE Trans. Biomed. Circuits Syst.*, vol. 5, no. 2, pp. 147–159, Apr. 2011.
[41] S. Micera, J. DiGiovanna, A. Berthoz, A. Demosthenous, J. Guyot, K. Hoffmann, D. Merfeld, and M. Morari, "A closed-loop neural prosthesis for vestibular disorders," in *Proc. 10th Symp. Neural Netw. Appl. Electr. Eng.*, Sep. 23–25, 2010, pp. 27–30.

Nicolas S. Valentin was born in Bogotá, Colombia. He received the B.S. degree in electrical engineering from the California State Polytechnic University, Pomona, CA, USA, in 2009, and the M.S. degree in biomedical engineering from Johns Hopkins University, Baltimore, MD, USA, in 2012. His graduate research work in the Vestibular Neuroengineering Laboratory at Johns Hopkins University focused on the development of a multichannel prosthesis prototype for restoration of vestibular function.

He is currently a Systems Engineer for Labyrinth Devices, Baltimore, MD, USA, working on the design and commercialization of the human-implantable vestibular prosthesis.

Kristin N. Hageman received the B.S. degree in biomedical engineering from Case Western Reserve University, Cleveland, OH, USA, in 2011, with a specialty in bioelectrical engineering. She is currently working toward the Ph.D. degree in biomedical engineering at Johns Hopkins University School of Medicine, Baltimore, MD, USA. Her research in the Vestibular NeuroEngineering Lab focuses on the circuit development of the next generation multichannel vestibular prosthesis.

Chenkai Dai received the M.D. and M.S. degrees from Tongji Medical College, Huazhong University of Science and Technology, Wuhan, China (1995–2003), and the Ph.D. degree in bioengineering from the University of Oklahoma, Norman, OK, USA, in 2008, where his research focused on middle ear mechanics.

He is a Research Associate in the Department of Otolaryngology-Head and Neck Surgery at the Johns Hopkins School of Medicine, Baltimore, MD, USA. His current research focuses on vestibular neurophysiology and on assessment and refinement of vestibular prosthesis technology in alert, behaving animals.

Charles C. Della Santina received the Ph.D. degree in bioengineering, in 1994, from the University of California, Berkeley, CA, USA, where his work focused on development of micromachined silicon devices for chronic multi-unit interfacing to the auditory/vestibular nerve, and the M.D. degree from the University of California, San Francisco, CA, USA, in 1997. He completed residency at the Johns Hopkins School of Medicine, Baltimore, MD, USA, in 2002.

He has been a clinician-scientist at Johns Hopkins, where he is Director of the Johns Hopkins Vestibular NeuroEngineering Lab and a Professor of Otolaryngology—Head & neck Surgery and Biomedical Engineering. His research focuses on vestibular neurophysiology and development of a vestibular prosthesis for restoration of labyrinthine sensation. He holds a founding interest in Labyrinth Devices LLC.

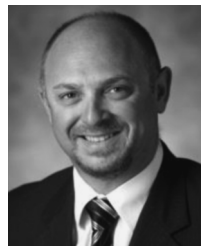

Gene Y. Fridman (M'13) received the B.S. degree in computer engineering from The University of Kansas, Lawrence, KS, USA, in 1992, the M.S. degree in electrical engineering from Purdue University, West Lafayette, IN, USA, in 1995, and the Ph.D. degree in biomedical engineering, specializing in neural recording and stimulation, and micro-electro-mechanical systems from the University of California, Los Angeles, CA, USA, in 2006, and then completed postdoctoral training at Johns Hopkins University, Baltimore, MD, USA, in 2009.

Prior to receiving the Ph.D. degree, he worked in the industry for five years in R&D as software and systems engineer before deciding to engage in an academic career. He is an Assistant Professor of Otolaryngology Head and Neck Surgery at the Johns Hopkins School of Medicine. His research focuses on stimulation and recording interaction with the nervous system for the innovation and improvement of the neuro-electronic prostheses including cortical, cochlear, and vestibular implants.